Squid Cartilage-Derived Carbon Quantum Dots for Selective Fluorescence Sensing of Hexavalent Chromium in Water

Abhinav Sobti[1]*

Received August 14, 2026
Accepted October 31, 2026
Electronic access November 15, 2026

The detection of hexavalent chromium (Cr(VI)) in water remains a significant analytical challenge due to its high toxicity, widespread industrial origin and high solubility, which facilitates rapid dispersion in aquatic systems. In the present study, carbon quantum dots (CQDs) were synthesized through a hydrothermal process using squid cartilage derived from *Uroteuthis duvaucelii*. The SC-CQDs were prepared by hydrothermal treatment at 200 °C for 8 h, followed by filtration and dialysis, and chromyl chloride (CrO_2Cl_2) was used as the Cr(VI) precursor in the sensing experiments. The resulting squid cartilage–derived CQDs (SC-CQDs) exhibit an average particle size of 4.28 ± 0.99 nm and are readily dispersible in aqueous media. Microscopic and spectroscopic characterisations reveal the formation of nanoscale carbon frameworks enriched with oxygenated surface functionalities, together with partially ordered carbon domains. The SC-CQDs exhibit excitation-dependent photoluminescence, along with a measurable dependence on solution pH and a fluorescence lifetime of approximately 4.3 ns. The fluorescence response of the SC-CQDs was evaluated in the presence of several potentially interfering ionic species, with aqueous Cr(VI) producing the greatest quenching response under the tested conditions. Increasing Cr(VI) concentration produced concentration-dependent fluorescence quenching, with a linear response in the lower concentration range and an estimated detection limit of approximately 5.4 μM. Although these results demonstrate a proof-of-concept Cr(VI)-responsive fluorescent material, further work is required to establish the quenching mechanism, assess performance in complex environmental matrices, and determine suitability for field-deployable sensing.

Keywords: Carbon quantum dots; Squid cartilage (*Uroteuthis duvaucelii*); Hydrothermal synthesis; Photoluminescence quenching; Hexavalent chromium (Cr(VI)); Marine biowaste.

Introduction

Heavy-metal contamination of water remains a major environmental concern, particularly in regions affected by industrial discharge. Among these contaminants, hexavalent chromium (Cr(VI)) is of particular concern because of its high aqueous solubility, mobility, and well-documented toxicity. Cr(VI) contamination is associated with industrial activities including electroplating, leather processing, textile manufacturing, and pigment production, while exposure has been linked to oxidative stress and carcinogenic effects[1,2]. Consequently, reliable detection of Cr(VI) at low concentrations is important for environmental monitoring and water-quality assessment.

Established chromium-analysis methods include atomic absorption spectroscopy and inductively coupled plasma-based techniques, which provide high analytical sensitivity but generally require specialized instrumentation, controlled laboratory conditions, and trained operators. Fluorescence-based sensing has therefore attracted interest as a complementary approach because optical responses can be measured rapidly and with comparatively simple sample handling[3,4].

Carbon quantum dots (CQDs) are water-dispersible fluorescent carbon nanomaterials whose emission can be influenced by particle structure, surface states, functional groups, excitation wavelength, and solution environment[5,6]. Their surface chemistry is strongly dependent on precursor composition and synthesis conditions, enabling interactions with target analytes to be tuned. Numerous CQD platforms have consequently been investigated for Cr(VI) detection, with reported mechanisms including static quenching, dynamic interactions, resonance-energy-transfer processes, and inner-filter effects.

Biomass-derived CQDs are of particular interest because biological and waste-derived precursors provide chemically diverse carbon-containing feedstocks. Recent studies have reported Cr(VI)-responsive carbon dots derived from seaweed, *Ruta graveolens* leaves, banana stem, flax straw, and other renewable precursors[7–10]. Squid gladius/cartilage contains carbon-rich structural biopolymers, including β-chitin and proteoglycan-associated components, but its use as a precursor for Cr(VI)-responsive CQDs has not, to our knowl-

[1] *Dubai College, United Arab Emirates*
* *Corresponding author: abhisobti100@gmail.com*

© The National High School Journal of Science 2026

edge, been reported. Additional primary studies have reported Cr(VI)-responsive carbon dots prepared from chitosan, *Poria cocos* polysaccharide, groundnuts, kelp, thymidine, and synthetic carbon/nitrogen precursors, demonstrating that precursor chemistry, surface composition, and spectral overlap can substantially influence sensitivity and quenching behaviour[11–16].

Recent studies have extended biomass-based Cr(VI) sensing through control of synthesis conditions. Solvent-controlled spinach-derived carbon dots achieved a detection limit of 0.242 μM[17]. *Lycium barbarum*-derived CQDs further demonstrate the use of plant feedstocks for fluorescence-based Cr(VI) detection[18].

Hydrothermally synthesized biowaste-derived carbon dots have also been investigated as selective Cr(VI) nanoprobes[19]. Other CQD systems combine Cr(VI) detection with optical thermometry, illustrating the influence of measurement conditions on fluorescence responses[20]. Nitrogen-doped carbon dots prepared from *Pueraria* residues provide another route for converting agricultural residues into Cr(VI)-responsive materials[21]. Kitchen-waste-derived oxygen-doped CQDs have additionally been applied to Cr(VI) detection in environmental water matrices, extending evaluation beyond simple aqueous standards[22].

Fish-scale-derived carbon dots used for glutathione sensing demonstrate the broader potential of fish-processing by-products as fluorescent precursors[23]. Carbon dot/chitin nanocrystal hybrids have also combined metal-ion detection with removal, supporting interest in chitin-containing materials for water treatment[24].

Beyond precursor selection, surfactant encapsulation of nitrogen-doped carbon dots has been explored to improve optical properties for Cr(VI) sensing[25]. Sulphur-doped carbon dots responsive to both Cr(VI) and Fe^{3+} highlight the importance of assessing competing-ion responses[26]. Carbon dot–cadmium sulfide composites exhibit Cr(VI)-induced quenching attributed to the inner-filter effect[27]. Combined inner-filter and dynamic-quenching contributions have also been reported, reinforcing the need for absorption and lifetime measurements before assigning a mechanism[28].

Alternative readouts include Cr(VI)-dependent emission shifts in pepitas-derived carbon dots, extending sensing beyond fluorescence-intensity changes[29]. Waste-biomass-derived carbon dots have also enabled semi-quantitative visual detection of Cr(VI) and Fe^{3+} [30]. Biological-matrix-derived carbon dots have further been incorporated into visual Cr(VI) detection kits[31]. Together, these studies identify sensitivity, interference control, mechanistic validation, and practical readout as benchmarks for evaluating new biomass-derived probes.

This study therefore investigates squid cartilage as an alternative marine-biowaste precursor for fluorescent carbon nanomaterials. The resulting SC-CQDs were characterized by HR-TEM, AFM, XRD, Raman spectroscopy, FT-IR, XPS, UV–visible spectroscopy, photoluminescence spectroscopy, and fluorescence-lifetime measurements. Their optical response to aqueous Cr(VI) was then evaluated as a proof-of-concept sensing application.

The objective is not to claim analytical superiority over established chromium methods, but to establish the material, quantify its fluorescence response under the tested conditions, and define the limitations that must be addressed before practical environmental deployment.

Materials and Methods

Materials

Fresh squid cartilage/gladius from *Uroteuthis duvaucelii* was obtained from a coastal fish market in Kochi, Kerala, India. All chemicals were analytical grade and were used as received.

Deionized (DI) water was used throughout synthesis and sensing experiments. Chromyl chloride (CrO_2Cl_2) was used as the Cr(VI) precursor. For the selectivity experiment, 5 μM test solutions containing Al^{3+}, As^{3+}, Ca^{2+}, Cd^{2+}, Cu^{2+}, Fe^{2+}, Na^{+}, Zn^{2+}, Pb^{2+}, and Cr(VI) were prepared from analytical-grade reagents.

Preparation of Squid Cartilage-Derived Carbon Quantum Dots

Fresh squid cartilage/gladius was washed repeatedly with water to remove adherent muscle tissue and surface impurities while retaining the structural matrix of the gladius. The cleaned material was dried under ambient conditions and subjected to controlled thermal treatment to obtain a fine carbon-containing precursor.

Squid gladius contains β-chitin and proteoglycan-associated organic components, providing a carbon-containing structural matrix for subsequent hydrothermal carbonization.

Approximately 2.5 g of the thermally treated precursor was dispersed in 50 mL of DI water and transferred to a 100 mL Teflon-lined stainless-steel autoclave. The autoclave was sealed and heated at 200 °C for 8 h under hydrothermal conditions. The resulting elevated-temperature, pressurized aqueous environment promoted conversion of the carbon-containing precursor into nanoscale carbonaceous products.

After hydrothermal treatment, the autoclave was allowed to cool naturally to room temperature (∼25 °C) before opening. A brown dispersion was obtained and processed immediately for purification.

© The National High School Journal of Science 2026

The dispersion was filtered through a syringe filter to remove larger particulate matter and subsequently dialyzed against DI water for 48 h to remove low-molecular-weight impurities and unreacted species. The purified dispersion was designated squid cartilage-derived carbon quantum dots (SC-CQDs) and stored at 4 °C until characterization and sensing experiments.

Storage at 4 °C was used as a standardized handling condition. Long-term storage stability and inter-batch reproducibility were not systematically quantified in the present study and are therefore treated as limitations rather than established performance characteristics.

Structural and Morphological Characterization

SC-CQD morphology was examined by high-resolution transmission electron microscopy (HR-TEM). Approximately ten individually resolved nanodots were measured from representative HR-TEM images for the reported size estimate, and the particle-size distribution was summarized as mean ± standard deviation (standard deviation obtained from Origin software).

Atomic force microscopy (AFM) was used to examine surface topography and representative height profiles; because a statistically robust multi-field AFM height distribution was not obtained, particle-size determination was based primarily on HR-TEM.

X-ray diffraction (XRD) was used to assess long-range structural order, while Raman spectroscopy was used to examine D- and G-band features associated with disordered and sp^2-rich carbon domains. The broad XRD feature and Raman intensity ratio were quantified from the recorded spectra.

Surface Chemical Analysis

Fourier-transform infrared (FT-IR) spectroscopy was used to identify major surface functional groups. X-ray photoelectron spectroscopy (XPS) was used to determine elemental composition and chemical-state assignments, with high-resolution fitting of the C 1s, O 1s, and Ca 2p regions.

Optical Characterization

UV–visible absorption and photoluminescence (PL) spectroscopy were used to characterize the optical response of the SC-CQDs. PL spectra were recorded over multiple excitation wavelengths (220–380 nm) to evaluate excitation-dependent emission. Fluorescence-lifetime measurements were also performed on the native SC-CQD dispersion.

The effect of pH on SC-CQD photoluminescence was evaluated over pH 2–12 by adjusting the dispersion with dilute acid or base and recording the corresponding emission spectra. These measurements characterize the pH dependence of the native SC-CQD fluorescence; a complete Cr(VI)-dependent pH/speciation study was not performed.

Relative fluorescence quantum yield was determined using quinine sulfate in 0.1 M H_2SO_4 as the reference standard ($\Phi_{st} = 0.54$).

Sample and standard solutions were excited at 360 nm, and quantum yield was calculated from $\Phi_x = \Phi_{st}\left(\frac{A_{st}}{A_x}\right)\left(\frac{I_x}{I_{st}}\right)\left(\frac{\eta_x^2}{\eta_{st}^2}\right)$, where A is absorbance, I is integrated fluorescence intensity, and η is solvent refractive index.

Fluorescence Sensing of Cr(VI) and Interfering Species

Chromyl chloride (CrO_2Cl_2) was used as the Cr(VI) precursor. In aqueous solution, Cr(VI) is present as pH-dependent oxyanion species rather than as a free Cr^{6+} cation; reported concentrations therefore refer to total molar Cr(VI), equivalent on a 1:1 chromium basis to the amount of CrO_2Cl_2 introduced.

For the selectivity experiment, the fluorescence response of SC-CQDs was measured after addition of 5 μM solutions of the tested ionic species (Al^{3+}, As^{3+}, Ca^{2+}, Cd^{2+}, Cr(VI), Cu^{2+}, Fe^{2+}, Na^{+}, Zn^{2+}, and Pb^{2+}). Each condition was measured in triplicate ($n = 3$), and error bars represent standard deviation. Cr(VI) titration spectra were recorded at $\lambda_{ex} = 320$ nm and quantified at 425 nm over an approximately 0–37.5 μM concentration range.

Fluorescence intensity in the absence of analyte was denoted I_0 and intensity after analyte addition was denoted I. The full I/I_0 response became nonlinear at higher Cr(VI) concentrations; therefore, quantitative fitting was restricted to the lower-concentration linear interval (approximately 5.0–12.5 μM). Fractional quenching, $(I_0 - I)/I_0$, followed the empirical relation $y = 11704.23815[C] - 0.02463$ ($R^2 = 0.993$), with [C] expressed in mol L^{-1}. The detection limit was calculated using LOD $= 3\sigma/S$, where σ is the standard deviation of the blank response and S is the calibration slope. No analyte-dependent absorbance correction or dedicated inner-filter-effect experiment was performed.

Results and Discussion

Morphological and Structural Characteristics of SC-CQDs

HR-TEM revealed predominantly quasi-spherical nanoscale particles. Measurement of approximately ten individually resolved particles yielded a mean diameter of 4.28 ± 0.99 nm. A representative high-resolution image showed lattice fringes with a spacing of approximately 0.21 nm. Because the particle count was limited, the measured distribution is treated as representative of the analyzed images rather than as a comprehensive population distribution.

© The National High School Journal of Science 2026

AFM imaging showed nanoscale surface features and corresponding line profiles. However, the AFM lateral features and line-height profile do not independently establish a 4.28 nm particle diameter. Accordingly, AFM is used here as qualitative topographic evidence, while the quantitative particle-size estimate is based on HR-TEM.

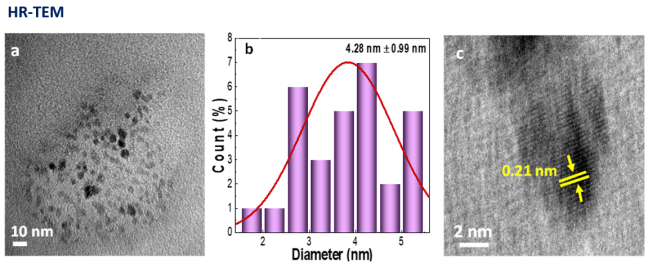


Figure. 1 HR-TEM images of SC-CQDs showing quasi-spherical nanoscale particles. The measured particle size was 4.28 ± 0.99 nm ($n \approx 10$).

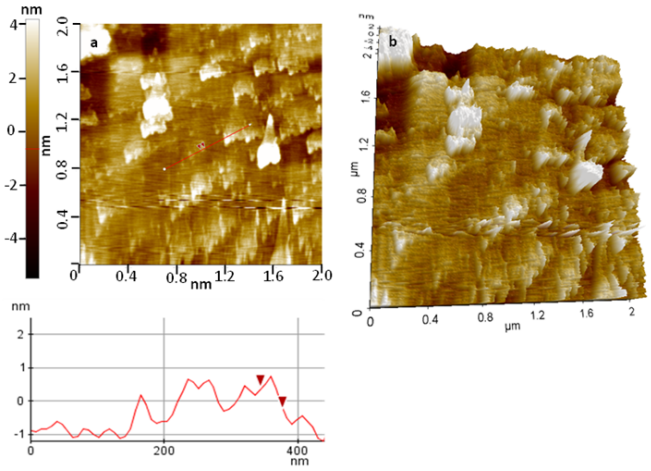


Figure. 2 AFM images and corresponding height profiles of SC-CQDs.

The microscopic observations are consistent with nanoscale carbonaceous particles containing localized ordered regions within a more disordered framework. At this length scale, both carbon-domain structure and surface functionality can influence optical behavior; mechanistic assignments are therefore considered together with the spectroscopic measurements below.

The XRD pattern exhibited a broad feature centered at approximately $2\theta = 22.12°$, indicating limited long-range crystalline order. Raman spectroscopy showed the characteristic D and G bands of disordered/sp^2-rich carbon, with an I_D/I_G ratio of approximately 1.1. Together, the XRD and Raman results support a predominantly disordered carbon structure containing short-range graphitic domains.

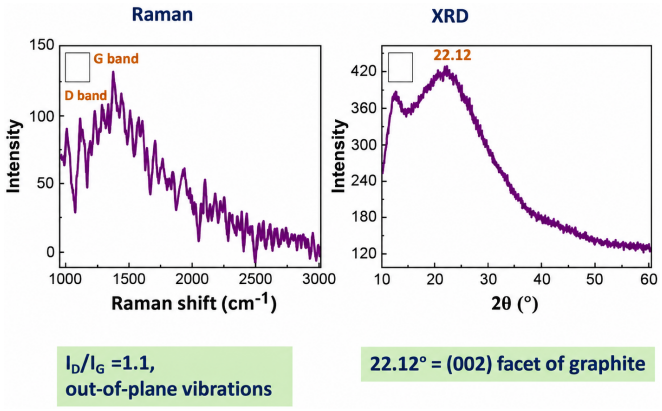


Figure. 3 Structural characterisation of SC-CQDs: (a) Raman spectrum showing the D and G bands, with an I_D/I_G ratio of approximately 1.1; (b) XRD pattern showing a broad diffraction feature centred at $2\theta = 22.12°$.

Taken together, HR-TEM, XRD, and Raman analysis support the formation of nanoscale carbonaceous particles containing both ordered sp^2-rich regions and structural disorder. The characterization supports classification of the product as a carbon-dot-like fluorescent nanomaterial; however, direct carbon mass-balance, CHNS/TOC, TGA, and precursor-control experiments were not performed and should be included in future work to strengthen attribution of the final carbon specifically to residual squid-derived carbon after the pre-hydrothermal thermal-treatment step.

Surface Chemical Composition

FT-IR spectroscopy indicated oxygen-containing surface functionality, with bands assigned to hydroxyl-containing groups together with C–O/C–O–C, C=O, and C=C-related vibrations. These functionalities are consistent with a polar, oxygenated surface that can support aqueous dispersibility. Their specific role in Cr(VI) quenching cannot be established from FT-IR alone.

XPS confirmed carbon, oxygen, and calcium in the analyzed material. The C 1s fit contained components assigned to C=C/C–C (∼284.7 eV), C–O–C (∼286.18 eV), and O–C=O (∼288.1 eV). The O 1s region contained a component near 533.75 eV assigned to C–O–C-type oxygen, while Ca 2p components were observed near 348.45 and 351.01 eV. The calcium signal is consistent with residual calcium-containing species from the biological precursor; the present data do not establish whether these species are incorporated within the carbonaceous nanostructure, exist as separate mineral phases, or remain surface-associated.

© The National High School Journal of Science 2026

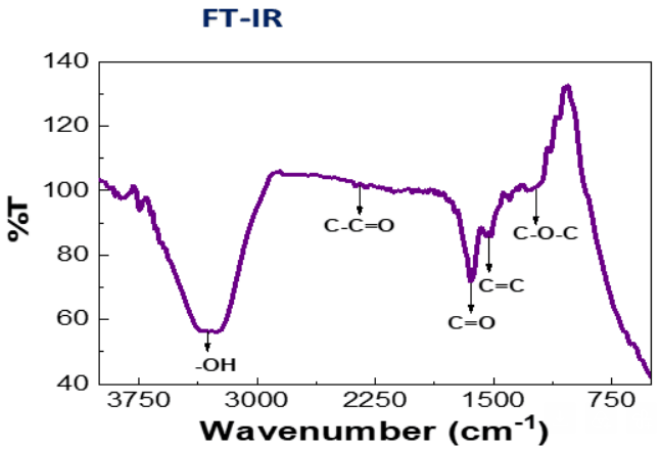


Figure. 4 FT-IR spectrum of SC-CQDs showing characteristic surface functional groups.

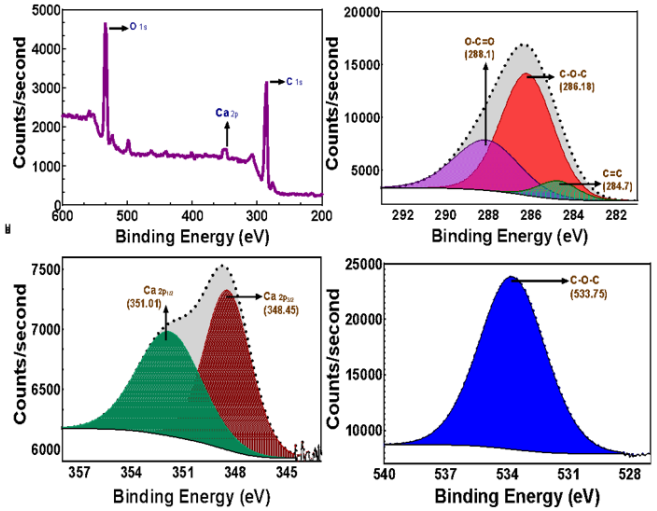


Figure. 5 XPS analysis of SC-CQDs: (a) survey spectrum; (b–d) high-resolution spectra of the C 1s, Ca 2p, and O 1s regions.

Optical Properties and Photoluminescence Behaviour

The UV–visible absorption spectrum showed prominent absorption in the UV region. Features in approximately the 230–260 nm range are consistent with π–π^* transitions associated with conjugated carbon domains, while absorption in approximately the 290–320 nm range is consistent with n–π^* transitions involving oxygen-containing surface groups.

Photoluminescence spectra recorded at excitation wavelengths from 220 to 380 nm showed excitation-dependent changes in emission position and intensity, indicating the presence of multiple emissive environments rather than a single uniform emissive state.

The native SC-CQD dispersion exhibited a fluorescence

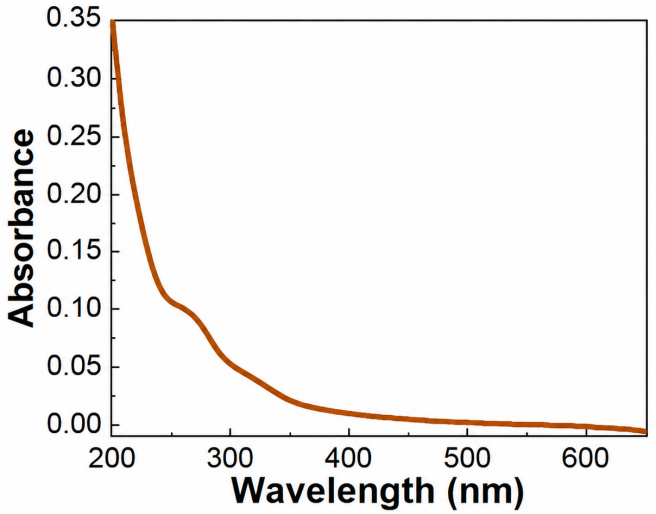


Figure. 6 UV–visible absorption spectrum of SC-CQDs showing absorption features in the 230–260 nm and 290–320 nm regions.

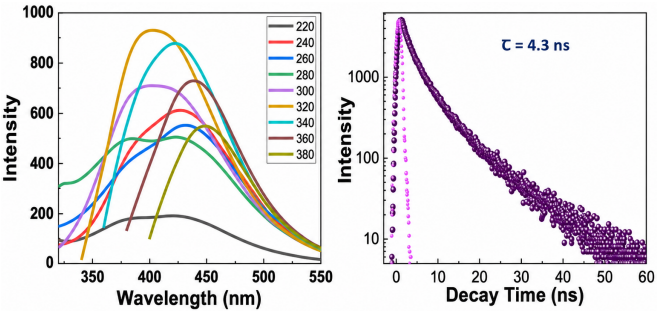


Figure. 7 Photoluminescence characteristics of SC-CQDs: (a) fluorescence emission spectra and (b) fluorescence lifetime measurement, with a measured lifetime of approximately 4.3 ns.

lifetime of approximately 4.3 ns. This value characterizes the excited-state decay of the unexposed material but does not, by itself, distinguish core-state emission from surface-state emission or establish the mechanism of Cr(VI)-induced quenching.

SC-CQD photoluminescence varied systematically across pH 2–12, confirming that the emissive response is sensitive to solution protonation conditions. This behavior is consistent with protonation/deprotonation of oxygen-containing surface functionalities and associated changes in emissive surface environments.

Because aqueous Cr(VI) speciation is itself pH dependent, the pH effect cannot be attributed solely to protonation of the SC-CQD surface. The present study did not systematically determine Cr(VI)-quenching efficiency across the full pH range; therefore, an optimum sensing pH is not assigned here.

Future studies should evaluate both CQD surface charge and chromate/hydrogen-chromate/dichromate speciation un-

© The National High School Journal of Science 2026

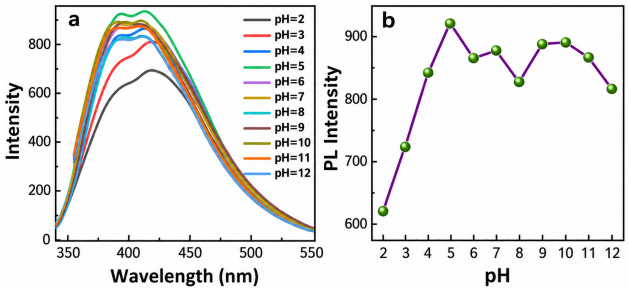


Figure. 8 Effect of solution pH on the photoluminescence of SC-CQDs over the tested pH range of 2–12.

der controlled pH conditions.

Selectivity among Tested Ionic Species

At a fixed analyte concentration of 5 μM, aqueous Cr(VI) produced the largest decrease in normalized fluorescence intensity among the tested species. The comparison included Al^{3+}, As^{3+}, Ca^{2+}, Cd^{2+}, Cu^{2+}, Fe^{2+}, Na^{+}, Zn^{2+}, and Pb^{2+}, with measurements performed in triplicate and plotted as mean $\pm$ SD.

Several non-target species nevertheless produced measurable quenching. The present experiment therefore demonstrates a preferential response to Cr(VI) under single-analyte conditions rather than absolute selectivity. Competitive-ion mixture experiments are required before selectivity can be claimed for chemically complex environmental samples.

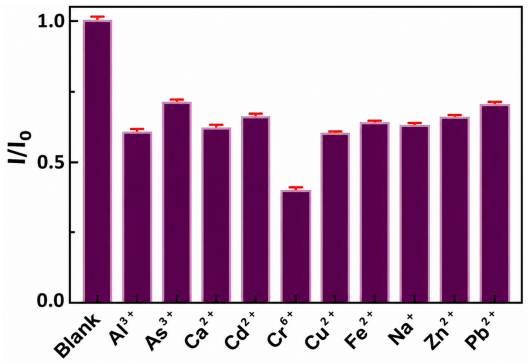


Figure. 9 Fluorescence response of SC-CQDs in the presence of 5 μM solutions of the tested ionic species. I_0 and I represent the fluorescence intensities at 425 nm in the absence and presence of the tested species, respectively ($\lambda_{ex} = 320$ nm).

Quantitative Cr(VI) Response and Mechanistic Considerations

Increasing total Cr(VI) concentration produced progressive quenching of SC-CQD fluorescence. The full response deviated from linearity at higher concentrations and approached a plateau; therefore, calibration was restricted to the lower-concentration interval. Fractional quenching, $(I_0 - I)/I_0$, was linear over approximately 5.0–12.5 μM and followed $y = 11704.23815[C] - 0.02463$ with $R^2 = 0.993$. Using LOD $= 3\sigma/S$, the estimated detection limit was 5.4 μM.

This empirical fractional-quenching calibration is reported without describing it as a Stern–Volmer plot; conventional Stern–Volmer analysis would require I_0/I versus quencher concentration.

The experiments establish concentration-dependent fluorescence quenching after addition of aqueous Cr(VI), but they do not permit definitive assignment of the quenching mechanism. Possible contributions include static or dynamic interactions with SC-CQD surface sites and absorption-related inner-filter effects.

Fluorescence lifetime was measured only for the native SC-CQDs and was not repeated after Cr(VI) addition, while analyte absorbance and spectral-overlap corrections were not independently evaluated. Mechanistic interpretations are therefore considered tentative. The current assay also requires laboratory fluorescence spectroscopy; field deployability has not been demonstrated.

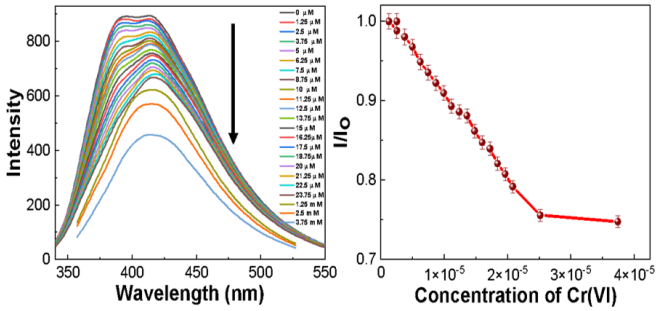


Figure. 10 Concentration-dependent fluorescence response of SC-CQDs to Cr(VI): (a) fluorescence spectra recorded at different Cr(VI) concentrations ($\lambda_{ex} = 320$ nm); (b) fluorescence-intensity ratio as a function of Cr(VI) concentration.

Comparison with Reported Cr(VI) Sensing Systems

Published CQD-based Cr(VI) sensors span a wide range of precursor chemistries, analytical ranges, and detection limits. To avoid generalized performance categories, Table 1 compares the present SC-CQD response with individual peer-reviewed studies using reported quantitative metrics.

The SC-CQD LOD is higher than several optimized or doped CQD systems; accordingly, the present contribution is framed primarily as proof-of-concept use of squid cartilage/gladius as a fluorescent carbon precursor rather than as a superior analytical sensor.

© The National High School Journal of Science 2026

Table 1 Comparison with selected published CQD-based Cr(VI) fluorescence sensors

Sensor	Linear range (μM)	LOD (μM)	Reference
Thymidine-derived N-CDs	0.1–430	0.00126	Ming et al., 2019
Poria cocos-derived CDs	1–100	0.25	Huang et al., 2022
Chitosan-derived CDs	1–400	0.59	Feng et al., 2022
Hydrothermal CDs	1–125	0.60	Hahn et al., 2024

Conclusion

Squid-cartilage/gladius-derived precursor material was converted into fluorescent nanoscale carbonaceous particles by hydrothermal treatment at 200 °C for 8 h. HR-TEM yielded a mean particle diameter of 4.28 ± 0.99 nm, while XRD and Raman spectroscopy indicated a predominantly disordered carbon structure containing short-range sp^2-rich domains. FT-IR and XPS showed an oxygenated surface together with a detectable calcium contribution from the biological precursor.

The SC-CQDs exhibited excitation-dependent photoluminescence, a native fluorescence lifetime of approximately 4.3 ns, and pH-dependent emission. In sensing experiments, aqueous Cr(VI) produced the largest quenching response among the tested ionic species, and concentration-dependent quenching yielded an estimated LOD of 5.4 μM. Because measurable responses were also observed for some non-target species and competitive-ion mixtures were not tested, the current data support a preferential rather than exclusive Cr(VI) response.

The principal contribution of this study is the proof-of-concept use of squid cartilage/gladius as a marine-biowaste precursor for a fluorescent Cr(VI)-responsive nanomaterial. The present work does not establish the detailed quenching mechanism, field deployability, real-water recovery, long-term stability, inter-batch reproducibility, or environmental life-cycle performance. Future studies should include precursor carbon-balance/control experiments, analyte-dependent fluorescence-lifetime and absorption-overlap measurements, competitive-ion mixtures, spiked environmental-water recovery tests, and systematic optimization of quantum yield and analytical sensitivity.

References

1 J. Kotaś, Z. Stasicka, Chromium occurrence in the environment and methods of its speciation. Environmental Pollution. Vol. 107, pg. 263–283, 2000, https://doi.org/10.1016/S0269-7491(99)00168-2.

2 M. Costa, Potential hazards of hexavalent chromate in our drinking water. Toxicology and Applied Pharmacology. Vol. 188, pg. 1–5, 2003, https://doi.org/10.1016/S0041-008X(03)00011-5.

3 M. Hahn, M. Jang, Y. Cho, M. Bae, M. Y. Han, Y. Piao, Fluorometric carbon-dots nanosensor for the detection of hexavalent chromium in water. Optical Materials. Vol. 147, pg. 114642, 2024, https://doi.org/10.1016/j.optmat.2023.114642.

4 S. Zhu, Y. Song, X. Zhao, J. Shao, J. Zhang, B. Yang, The photoluminescence mechanism in carbon dots (graphene quantum dots, carbon nanodots, and polymer dots): current state and future perspective. Nano Research. Vol. 8, pg. 355–381, 2015, https://doi.org/10.1007/s12274-014-0644-3.

5 S. N. Baker, G. A. Baker, Luminescent carbon nanodots: emergent nanolights. Angewandte Chemie International Edition. Vol. 49, pg. 6726–6744, 2010, https://doi.org/10.1002/anie.200906623.

6 S. Y. Lim, W. Shen, Z. Gao, Carbon quantum dots and their applications. Chemical Society Reviews. Vol. 44, pg. 362–381, 2015, https://doi.org/10.1039/C4CS00269E.

7 H. Tian, G. Ju, M. Li, W. Fu, Y. Dai, Z. Liang, Y. Qiu, Z. Qin, X. Yin, Fluorescent 'on-off-on' sensor based on N,S co-doped carbon dots from seaweed (Sargassum carpophyllum) for specific detection of Cr(VI) and ascorbic acid. RSC Advances. Vol. 11, pg. 35946–35953, 2021, https://doi.org/10.1039/D1RA06544K.

8 B. K. John, N. John, S. Mathew, B. K. Korah, M. S. Punnoose, B. Mathew, Fluorescent carbon quantum dots as a novel solution and paper strip-based dual sensor for the selective detection of Cr(VI) ions. Diamond and Related Materials. Vol. 126, pg. 109138, 2022, https://doi.org/10.1016/j.diamond.2022.109138.

9 J. Goswami, S. S. Rohman, A. K. Guha, P. Basyach, K. Sonowal, S. P. Borah, L. Saikia, P. Hazarika, Phosphoric acid assisted synthesis of fluorescent carbon dots from waste biomass for detection of Cr(VI) in aqueous media. Materials Chemistry and Physics. Vol. 286, pg. 126133, 2022, https://doi.org/10.1016/j.matchemphys.2022.126133.

10 G. Hu, L. Ge, Y. Li, M. Mukhtar, B. Shen, D. Yang, J. Li, Carbon dots derived from flax straw for highly sensitive and selective detections of cobalt, chromium, and ascorbic acid. Journal of Colloid and Interface Science. Vol. 579, pg. 96–108, 2020, https://doi.org/10.1016/j.jcis.2020.06.034.

11 Y. Feng, R. Li, P. Zhou, C. Duan, Non-toxic carbon dots fluorescence sensor based on chitosan for sensitive and selective detection of Cr(VI) in water. Microchemical Journal. Vol. 180, 107627, 2022, https://doi.org/10.1016/j.microc.2022.107627.

12 Q. Huang, Q. Bao, C. Wu, M. Hu, Y. Chen, L. Wang, W. Chen, Carbon dots derived from Poria cocos polysaccharide as an effective 'on-off' fluorescence sensor for chromium(VI) detection. Journal of Pharmaceutical Analysis. Vol. 12, pg. 104–112, 2022, https://doi.org/10.1016/j.jpha.2021.04.004.

13 V. Roshni, S. Misra, M. K. Santra, D. Ottoor, One pot green synthesis of C-dots from groundnuts and its application as Cr(VI) sensor and in vitro bioimaging agent. Journal of Photochemistry and Photobiology A: Chemistry. Vol. 373, pg. 28–36, 2019, https://doi.org/10.1016/j.jphotochem.2018.12.028.

14 S. Feng, Z. Gao, H. Liu, J. Huang, X. Li, Y. Yang, Feasibility of detection valence speciation of Cr(III) and Cr(VI) in environmental samples by spectrofluorimetric method with fluorescent carbon quantum dots. Spectrochimica Acta Part A: Molecular and Biomolecular Spectroscopy. Vol. 212, pg. 286–292, 2019, https://doi.org/10.1016/j.saa.2018.12.055.

15 F. Ming, J. Hou, C. Hou, M. Yang, X. Wang, J. Li, D. Huo, Q. He, One-step synthesized fluorescent nitrogen-doped carbon dots from thymidine for Cr(VI) detection in water. Spectrochimica Acta Part A: Molecular and Biomolecular Spectroscopy. Vol. 222, 117165, 2019, https://doi.org/10.1016/j.saa.2019.117165.

16 D. Das, R. K. Dutta, N-Doped carbon dots synthesized from ethylene glycol and β-alanine for detection of Cr(VI) and 4-nitrophenol via photoluminescence quenching. ACS Applied Nano Materials. Vol. 4, pg. 3444–3454, 2021, https://doi.org/10.1021/acsanm.0c03329.

17 S. Wang et al., Preparation of Multicolor Biomass Carbon Dots Based on

Solvent Control and Their Application in Cr(VI) Detection and Advanced Anti-Counterfeiting. ACS Omega. Vol. 8, pp. 6550–6558, 2023, https://doi.org/10.1021/acsomega.2c06942.

18 J. Xie, Z. Wu, J. Sun, C. Lv, Q. Sun, Green Synthesis of Carbon Quantum dots Derived from Lycium barbarum for Effective Fluorescence Detection of Cr(VI) Sensing. Journal of Fluorescence. Vol. 34, pp. 571–578, 2024, https://doi.org/10.1007/s10895-023-03300-5.

19 A. Ghosh, B. Boro, S. S. Chowdhury, R. Ranjan, N. Dasgupta, S. Ranjan, Ultrasensitive and Selective Detection of Chromium(VI) Using Biowaste Derived Fluorescent Nanoprobes of Hydrothermally Synthesized Carbon-Dots. ChemistrySelect. Vol. 9, e202404198, 2024, https://doi.org/10.1002/slct.202404198.

20 A. Kumar, Ritu, I. Kumar, S. Kumar, A. K. Gathania, Eco-friendly carbon quantum dots as a bi-functional fluorescent probe for Cr(VI) detection and optical thermometry. Materials Research Bulletin. Vol. 187, 113394, 2025, https://doi.org/10.1016/j.materresbull.2025.113394.

21 Z. Zheng, Z. Zhou, Green Synthesis of Nitrogen-Doped Carbon Dots from Pueraria Residues for Use as a Sensitive Fluorescent Probe for Sensing Cr(VI) in Water. Sensors. Vol. 25, 5554, 2025, https://doi.org/10.3390/s25175554.

22 T. Mandal, R. N. Senapati, A. K. Ghosh, R. E. Masto, V. Singh, Kitchen Waste-Derived Oxygen-Doped Fluorescent Carbon Quantum Dots for Ultra-Trace Detection of Chromium(VI) in Environmental Water Matrices. ACS Sustainable Resource Management. Vol. 2, pp. 1786–1796, 2025, https://doi.org/10.1021/acssusresmgt.5c00310.

23 Y. Zhang, C. Lei, P. Dong, P. Fu, Y. Zhang, R. Hua, Green synthesis of carbon dots from fish scales for selective turn off–on detection of glutathione. RSC Advances. Vol. 14, pp. 3578–3587, 2024, https://doi.org/10.1039/D3RA07444G.

24 T. S. Ngo, C. T. Tracey, A. G. Navrotskaya, A. V. Bukhtiyarov, P. V. Krivoshapkin, E. F. Krivoshapkina, Reusable carbon dot/chitin nanocrystal hybrid sorbent for the selective detection and removal of Cr(VI) and Co(II) ions from wastewater. Carbohydrate Polymers. Vol. 304, 120471, 2023, https://doi.org/10.1016/j.carbpol.2022.120471.

25 Q. Chen, N. Li, Y. Tian, Q. Liu, X. Zou, M. Fan, Z. Gong, Surfactant encapsulating N-doped carbon dots with enhanced optical properties as a selective sensor for Cr(VI) detection. Analyst. Vol. 148, pp. 2818–2824, 2023, https://doi.org/10.1039/D3AN00517H.

26 A. G. Kolekar et al., Facile synthesis of sulphur-doped carbon dots (S-CDs) using a hydrothermal method for the selective sensing of Cr^{6+} and Fe^{3+} ions: application to environmental water sample analysis. RSC Advances. Vol. 14, pp. 3473–3479, 2024, https://doi.org/10.1039/D3RA07545A.

27 A. B. Patil, P. L. Chaudhary, P. V. Adhyapak, Carbon dots–cadmium sulfide quantum dots nanocomposite for 'on–off' fluorescence sensing of chromium(VI) ions. RSC Advances. Vol. 14, pp. 12923–12934, 2024, https://doi.org/10.1039/D4RA00436A.

28 H. Sun et al., IFE and Dynamic Quenching mediated fluorescent sensing of Cr(VI) based on nitrogen-doped biomass carbon dots. Environmental Research. Vol. 286, 123024, 2025, https://doi.org/10.1016/j.envres.2025.123024.

29 A. John, R. E. Roy, H. Hari, A. K. Zachariah, Emerging Stoke's Shift-Based Cr(VI) Fingerprint Sensor from Intensely Blue Fluorescent, High Quantum Yield, Pepitas-Derived Carbon Dots. ACS Applied Optical Materials. Vol. 2, pp. 291–300, 2024, https://doi.org/10.1021/acsaom.3c00411.

30 L. Xia et al., Sustainable and Green Synthesis of Waste-Biomass-Derived Carbon Dots for Parallel and Semi-Quantitative Visual Detection of Cr(VI) and Fe^{3+}. Molecules. Vol. 27, 1258, 2022, https://doi.org/10.3390/molecules27041258.

31 S. Liu, Y. Zhang, Y. Zhang, J. Zhang, R. Tian, L. Zhao, Visual fluorescence detection kit for Cr(VI) based on biological matrix-derived carbon dots and assisted for AA. Diamond and Related Materials. Vol. 148, 111382, 2024, https://doi.org/10.1016/j.diamond.2024.111382.

© The National High School Journal of Science 2026